Experimental Mechanics (2009) 49:257–275
DOI 10.1007/s11340-008-9166-9

Deformation and Failure Modes of I-Core Sandwich Structures Subjected to Underwater Impulsive Loads

L.F. Mori · D.T. Queheillalt · H.N.G. Wadley · H.D. Espinosa

Received: 27 March 2008 / Accepted: 26 June 2008 / Published online: 4 September 2008

Abstract This article reports an experimental study carried out with the aim of quantifying performance and failure modes of sandwich structures when subjected to impulsive blast loading. In particular, performance enhancement with respect to solid panels of equal mass per unit area is assessed. Likewise, the optimal distribution of the mass per unit area in the design of sandwich structures is investigated by comparing the behavior of sandwich structures with various distributions of face sheets thickness. By employing a previously developed FSI experiment, the study confirmed that usage of sandwich structures is beneficial and that performance enhancements, in terms of maximum panel deflection, as high as 68% are possible. The study also confirms theoretical and computational analyses suggesting that use of soft cores maximizes the benefits. Another interesting aspect revealed by this work is that the level of enhancement is highly related to the applied normalized impulse. The same distribution of mass per unit area between face sheets resulted in different normalized maximum deflection. A better performance enhancement was achieved at lower impulses. Here again, failure modes and their sequence seem to be the directly related to this finding. The work here reported clearly reveals a number of important features in the study of lightweight structures and points out to the synergies between structure geometry, materials, manufacturing methods, and threat levels as manifested by the strength of the impulse. Further theoretical and computational studies accounting for experimentally observed failure modes and its interdependence with the fabrication methods is needed to achieve additional predictive capabilities.

Keywords Fluid–structure interaction · Sandwich structures · Wave propagation · Dynamic plasticity · Moiré · Impact

L.F. Mori · H.D. Espinosa (✉, SEM member)
Department of Mechanical Engineering,
Northwestern University,
Evanston, IL 60208, USA
e-mail: espinosa@northwestern.edu

D.T. Queheillalt · H.N.G. Wadley
Department of Materials Science and Engineering,
University of Virginia,
Charlottesville, VA 22904, USA

Introduction

Liang et al. [1] studied theoretically and numerically the response of sandwich panels subjected to water blast. In particular, they analyzed the effect of fluid–structure interaction and water cavitation. Based on their analyses, they divided the structures into two categories: those with strong and with soft cores. The identification of strong versus soft cores was based on failure modes and transient load transfer characteristics within the structure including core buckling. Pyramidal and honeycomb cores were categorized as hard while I-cores were categorized as soft for certain dimensions and aspect ratios. They proposed soft-core designs for the best overall performance. In parallel studies, Hutchinson and co-workers [2, 3] extended the work by Fleck and Deshpande [4, 5] and suggested optimal design of sandwich plates to sustain impulsive pressure wave in air or water environments. They advanced the concept that optimally designed sandwich plates could sustain water shocks which are about two times larger than monolithic plates of the same mass per unit area and material. This work report a series of experiments based on these predictions with the scope of assessing their validity.

An experimental apparatus incorporating fluid–structure interaction (FSI) effects was recently developed to test scaled structures [6, 7]. The set-up allows characterization of the response of solid and sandwich structures subjected to underwater blast impulsive loading. Failure modes are identified by means of real time measurements of deflection profiles, pressure histories, and post-mortem plasticity and fracture analyses. The performance of the set-up was assessed by conducting calibration plate impact experiments, in lieu of underwater explosion, in which pressure sensors were employed to record pressure histories. The experiments confirmed that the FSI setup can generate an exponentially decaying pressure history. Shadow Moiré and high speed photography (using a Cordin Intensified CCD Camera 220-8 high-speed camera) were also employed to record in real time the full field out-of-plane deformation profile of the structures [6, 7].

Using the FSI experiment, solid panels and stainless steel sandwich panels with strong pyramidal and honeycomb cores were successfully investigated. The studies showed that sandwich panels can lead to a reduction in panel deflection, by as much as 30%, when compared to solid panels of equal mass per unit area [8, 9]. Likewise, comparison of computations, based on a continuous homogenized model for the core [9, 10], with experimentally identified panel deformation histories indicate that such models are accurate enough to be used in full scale structural design and assessment.

The work described in this article seeks to experimentally explore the validity of the soft core hypothesis using the water shock tube experimental apparatus. The manuscript is organized as follows. In the "Methods" section, the experimental set up is described and the pressure history and normalized impulse achieved in FSI experiments defined. In the "Experimental Results" section, the experimental results for three types of sandwich panels with I-core are reported. A performance comparison is given in the "Comparison of Performances" section and a discussion of results and their implications are provided in the "Concluding Remarks" section.

Methods

Experimental Setup

In this investigation we use the FSI setup first reported in [6]. In the experiment, a water chamber made of steel is incorporated into a gas gun apparatus as shown in Fig. 1. A scaled structure (specimen panel) is fixed at one end of the water chamber, which is sealed at the other end by a steel piston containing o-rings. A flyer plate impacts the piston and produces an exponentially-decaying pressure history that propagates into the water and imposes an impulse to the wet side of the specimen panel. In the study reported here, rather than directly bolting the specimen panels to the anvil tube [Fig. 1(a)], as in [6, 9], the specimen is clamped using a steel frame and a rubber ring [Fig. 1(b)].

Stainless steel panel structures with soft I-cores were subjected to water born shocks and compared to equivalent mass monolithic plates using a maximum panel deflection metric. The mass per unit area of the sandwich structures was governed by the face sheet thicknesses and the core relative density and was made identical to that of the solid panels. The tested sandwich panels had an I-core relative density of 2% (see Table 1). For each experiment, three loading parameters are of interest: the peak water pressure

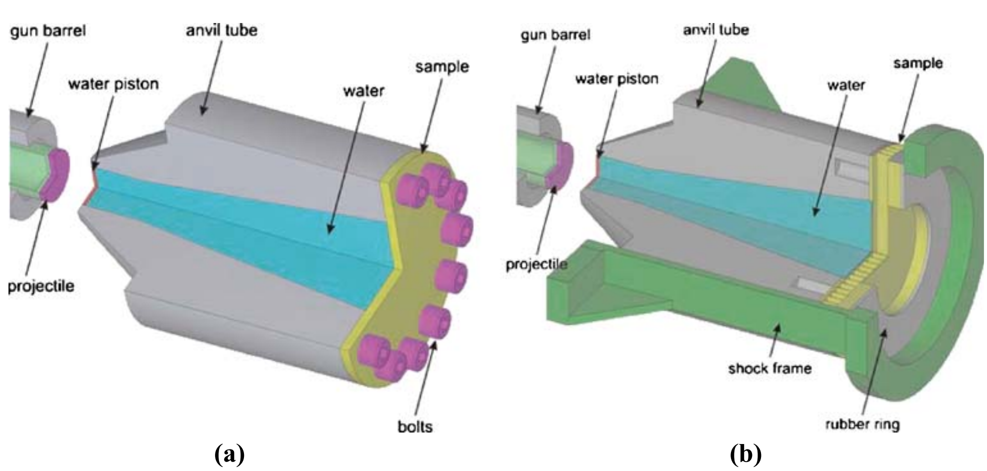

Fig. 1 Configuration of the water shock tube for the fluid–structure interaction experimental studies. (**a**) Case of bolted sample. (**b**) Case of specimen clamped using a steel frame and a rubber ring

Table 1 Properties of the test specimens

Structure type	Material	Core relative density (%)	Mass per unit area (kg/m^2)	Thickness (mm)
Soft-I-core sandwich	AISI 304 stainless steel	2	11.79	23.88

just ahead of the specimen panel (p_0), the characteristic decay time (t_0), and the far field applied impulse (I_0). The incident transient load can be idealized as an exponentially decaying pressure given by:

$$p = p_0 \times e^{-t/t_0} \tag{1}$$

where p_0 is the peak water pressure measured just in front of the specimen panel and t_0 is a characteristic decay time [10]. Equation (1) is derived using wave propagation theory with the assumption of linearity for the water equation of state.

In the FSI setup, the peak pressure p_0 is governed by the projectile impact velocity (V_0), the acoustic impedances of the piston (Z_s) and the fluid (Z_f) and by the experimental geometry, namely [9]:

$$p_0 = V_0 \times \left(\frac{D_i}{D}\right)^2 \times \frac{Z_s \times Z_f}{Z_s + Z_f}, \tag{2}$$

where D and D_i are the diameters of the water tube at the specimen and impact locations, respectively.

Likewise, the time constant t_0 is obtained from the evolution of the dimensionless pressure profile as a function of time:

$$\frac{p}{p_0} = e^{-t_n/t_0} = \left[\frac{Z_s \times Z_f}{Z_s + Z_f}\right]^n, \quad n = 0, 1, 2, \ldots \tag{3}$$

In this equation, n is the number of wave reverberations in the flyer plate and t_n is the corresponding elapsed time.

The far field impulse I_0 per unit area is given by:

$$I_0 = \sum_{n=0}^{\infty} p_0 \times \left[\frac{Z_s \times Z_f}{Z_s + Z_f}\right]^n \times \Delta t \approx p_0 \times t_0 \tag{4}$$

where Δt is the time required for the elastic longitudinal wave to transverse the flyer plate twice.

To compare the response of various structures subjected to different loadings, the non-dimensional impulse $\hat{I}$ introduced by Xue and Hutchinson [3] is used. $\hat{I}$ is defined as:

$$\hat{I} = \frac{I_0}{\overline{M} \times \sqrt{\sigma_y/\rho}} \tag{5}$$

where I_0 is the impulse per unit area previously defined, $\overline{M}$ the panel mass per unit area, σ_y the uniaxial tensile yield stress, and ρ the density of the material used to make the structure. All the specimens considered in this investigation were made of AISI 304 stainless steel with σ_y=205 MPa and ρ=7,900 kg/m^3.

Specimen Geometry and Boundary Conditions

In the investigation conducted on pyramidal truss core and square honeycomb core sandwich panels [9], the panels were rigidly clamped at the boundary, as shown in Fig. 2(a). With this boundary condition, introduced by Xue and Hutchinson [3], the sheet facing the water (wet face sheet) is clamped at the specimen periphery and therefore core crushing at the boundary is prevented. To implement such clamped boundary condition, the samples were bolted to the anvil tube with twelve 1″-8 cap screws [9]. Each hole made in the panel, to fit the screw, had a coaxial counter-bore on which steel solid-ring spacers, which prevented the crushing of the core. The experiments conducted with this configuration showed that the bolts did not completely eliminate in-plane radial displacement of the panel (due to slippage and hole ovalization) and that

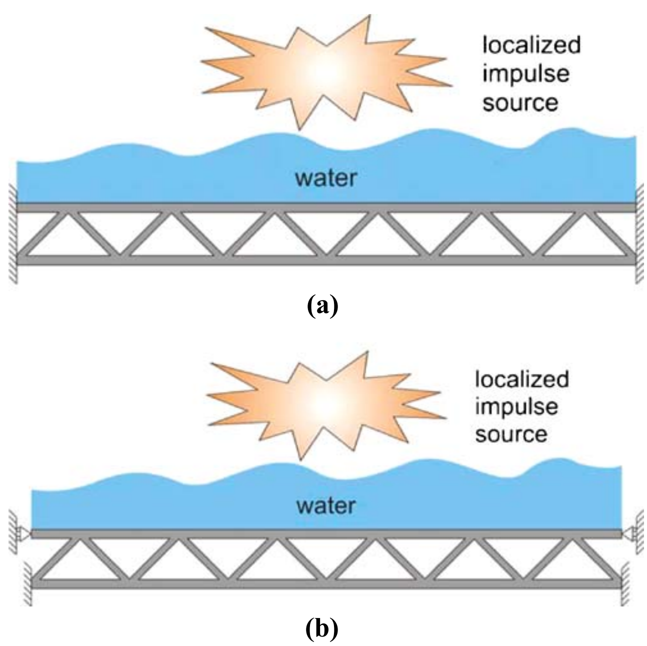

Fig. 2 Schematic of two boundary conditions implemented in the FSI experiments. The compliant gripping method is used for the first time in this investigation. (**a**) Edge clamped boundary condition. (**b**) Compliant boundary condition

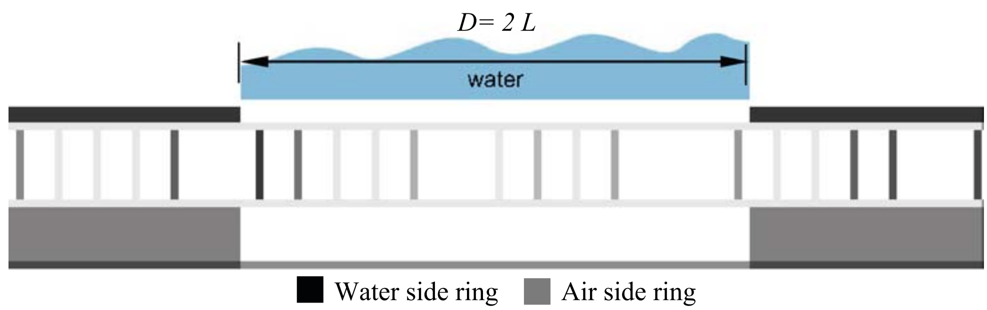

Fig. 3 Schematic drawing of a cross-section of the soft-I-core panels. The thickness of the face sheets and of the I-core plates is not at scale with the rest of the specimen. *L* is half the specimen span equal to 72.6 mm

most of the severe deformation of the core happens near the boundary [9]. To overcome these issues and to produce boundary conditions more realistic to naval applications, a compliant boundary condition introduced by Liang et al. [1] was implemented. The new boundary condition allows the sheet facing the water to freely move in the direction of the incident impulse while preventing the radial boundary displacement, Fig. 2(b).

In our practical implementation of such boundary condition, the face sheets were rigidly bonded to a pair of steel rings as shown in Fig. 3. The two rings have different masses (i.e., different thickness) with the ring bonded to the water face sheet being lighter (4.6 mm thick), and the one bonded to the air face sheet more massive (19 mm thick). The inertia of the thick ring prevents all displacements and rotations of the air face sheet (fixed boundary condition) and the overall boundary axial displacement of the entire panel. The thinner ring, on the water side, has an in-plane stiffness that prevents radial displacement of the water side face sheet, at the boundary, but allows the crashing of the core. The thickness of this plate requires optimization to achieve a high radial displacement constraint with minimum inertia in the impulse direction. The sandwich panels were clamped to the water anvil using a steel shock frame, Fig. 1(b). A thin hard rubber ring was placed between the frame and the panel to achieve a uniformly distributed contact pressure.

Three types of soft I-core panels were fabricated from AISI 304 stainless steel. The overall thickness for all of them was 23.88 mm. One type used equal thickness face sheets while the other two varied the front and back face sheet thickness as indicated in Fig. 4. The core relative density for all three panel types was 2% and their mass per unit area was also the same (11.79 kg/m^2). The material properties for AISI 304 stainless steel are reported in Table 2.

The I-core sandwich structures were fabricated from AISI 304 stainless steel by brazing. The spacing of the I-core members was achieved using a 304 stainless steel comb fixture, which maintained a regular spacing between members during the brazing process. A braze alloy with a nominal composition of Ni–22.0 Cr–6.0 Si, wt.% (Nicrobraz 31) was applied by spraying the surfaces to be bonded with a mixture of the braze powder and a polymer binder (Nicrobraz 520 cement) both supplied by Wal Colmonoy

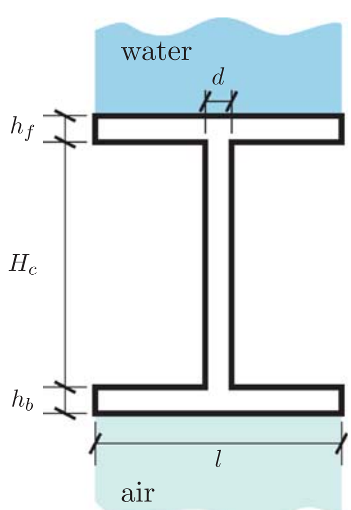

Dimension	Case I	Case II	Case III
h_f	0.508	0.762	0.254
h_b	0.508	0.254	0.762
H_c	22.86	22.86	22.86
l	12.7	12.7	12.7
d	0.258	0.258	0.258

All the dimensions are in millimeters.

Fig. 4 Geometry of the three types of tested I-core specimens

Table 2 Material properties for AISI 304 stainless steel

Quantity	Symbol	Unit	AISI 304 SS
Young's modulus	E	GPa	200
Poisson's ratio	ν	–	0.3
Density	ρ_0	kg/m^3	7,900
Yield stress	σ_y	MPa	205

(Madison Heights, WI). The air and water support ring components were also sprayed with the braze alloy/binder mixture and combined with the I-core sandwich structures forming the I-core assembly. The I-core assemblies were placed in a vacuum furnace at a base pressure of ~10^{-4} Torr. They were heated at 10°C/min to 550°C, held for 1 h (to volatilize the binder), then heated to the brazing temperature of 1,020°C. They were held for 60 min at this temperature before furnace cooling at ~25°C/min to ambient temperature. The brazed assemblies were water jet cut to a circular shape 29.2 cm in diameter. Figure 5 shows a schematic illustration of the I-core assembly process.

Experimental Results

Case I: Equal Thickness Face Sheets

The sandwich panel was tested using a flyer plate 4.84 mm thick launched at a velocity of 296 m/s. This resulted in a peak pressure p_0 of 76.7 MPa and a characteristic decay time t_0 of ~25.8 μs. The corresponding applied impulse I_0 was 36.17 N s and the non-dimensional applied impulse $\hat{I}$ was 1.045. Figure 1 shows photographs of the panel after testing. The maximum rear deflection was measured to be 11.66 mm and the non-dimensional maximum deflection, δ_{max}/L=0.153, where L=76.2 mm is half the specimen span. The final compressive strain of the crushed core was estimated at ε_c=87.5%.

Several distinct failure modes were observed in this experiment. The sandwich panel exhibited a different behavior between the front and the back face sheets. Differential plastic straining of the face sheet led to a slight imprint of the core webs on the dry and wet face sheets, Fig. 6(a) and (b). While the deformation of the back face sheet was homogeneous, as shown in Fig. 6(b) and (c), that of the front face sheet exhibited significant wrinkling, Fig. 6(a) and (d). A partial delamination occurred between the water face and the water ring, as shown in Fig. 6(d)–(f). The delamination did not extend over the whole water ring surface, which implies that the water ring–face sheet interface allowed some boundary rotation of the wet face sheet but constrained its displacement in the radial direction. As a result, the deformation of the core is not localized along the boundary but it is spread all over the specimen and in particular in the middle. Note that this behavior is quite different from the one obtained with the clamped boundary condition [9]. However, because of the water face sheet–water ring delamination, one can conclude that the boundary condition used in the numerical simu-

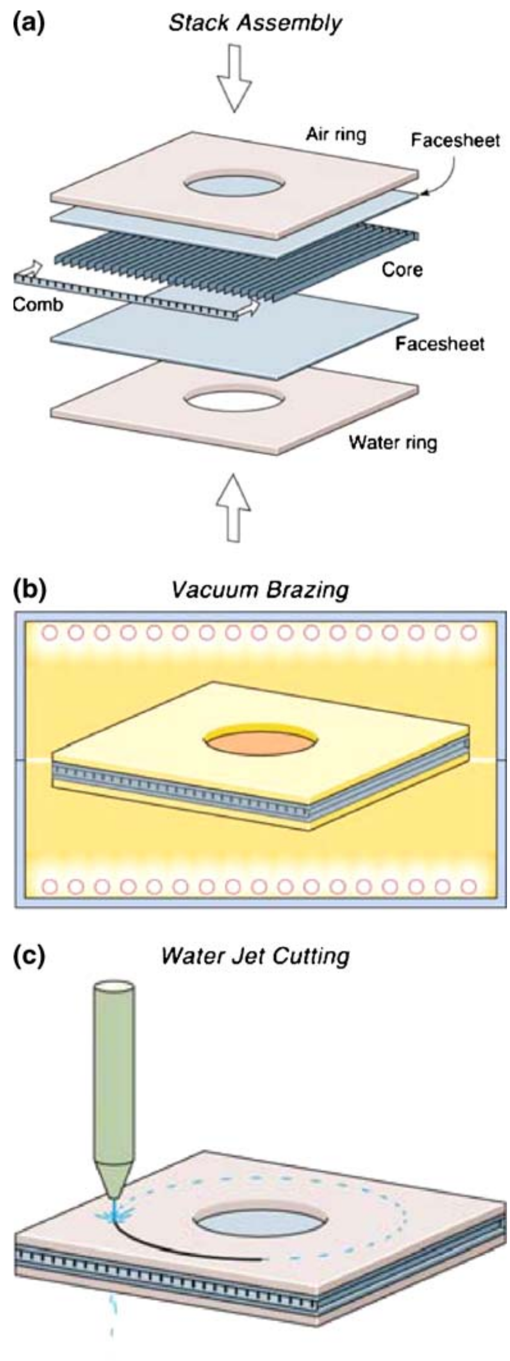

Fig. 5 Schematic illustrations of the I-core assembly process

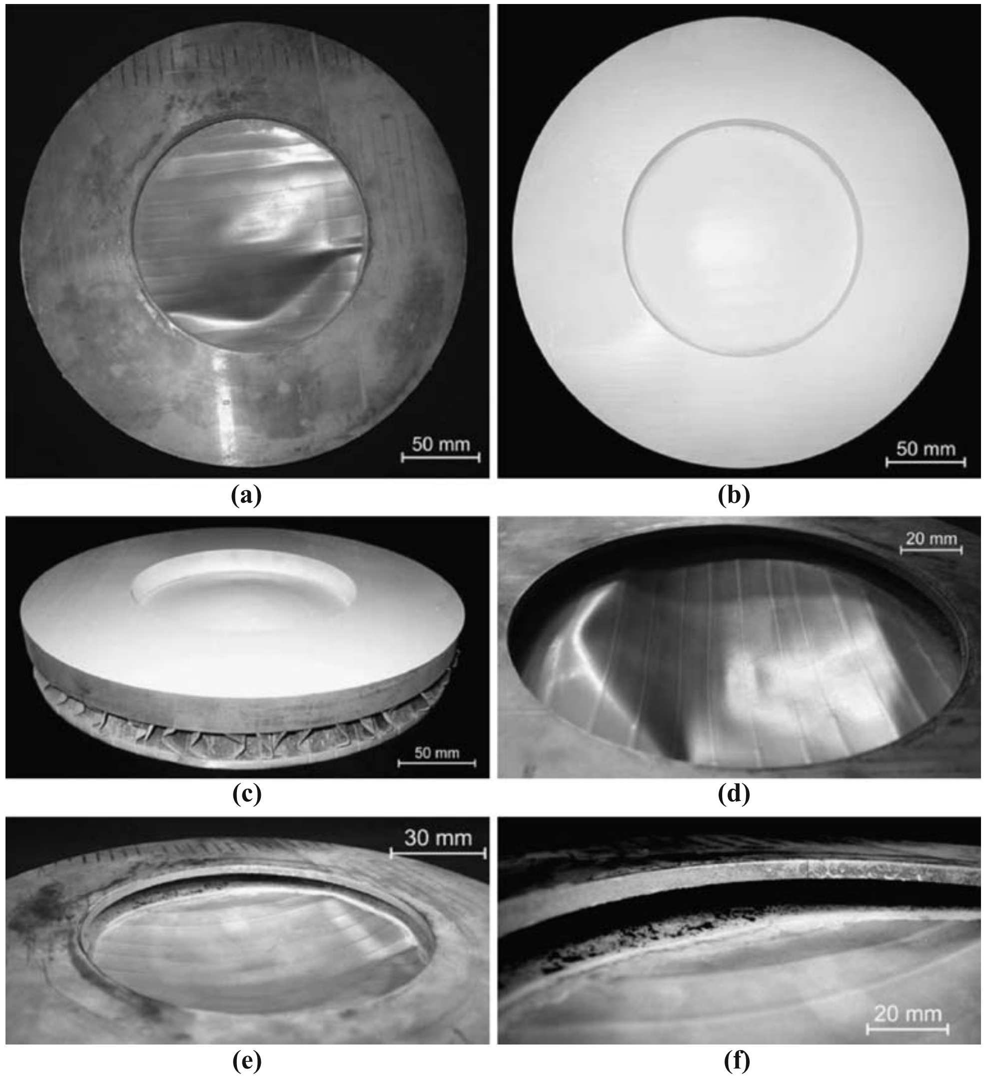

Fig. 6 Images of AISI 304 stainless steel sandwich panel with soft-I-core, case I (sheets of equal thickness), after impulsive loading; (**a**) and (**b**) show the front and the back of the face sheets; (**c**) shows a side view and (**d**)–(**f**) report delamination details. (**a**) Front (water side), (**b**) back (air side), (**c**) side, (**d**) detail of the front, (**e**) detail of the front, (**f**) detail of the front

lations reported in Liang et al. [1] were only partially achieved in the experiments.

After loading, the panel was sectioned using a water jet cutting method. The resulting cross section is shown in Fig. 7(a). In contrast to the setup with clamped boundary condition [9], the deformation of the core is spread all over the panel with significant core crushing between the two rings. Figure 7(b) and (c) illustrate the failure modes of the I-core as a function of the radial coordinate. Figure 7(b) also provides the spatial variation of the I-webs buckling: at the periphery (on the left) the core is only partially deformed (early stage of buckling) while in the middle (on the right) is completely crushed (late stage of buckling). The post mortem front and back face sheets profiles along the diameter of the panel are reported in Fig. 7(d). While deformation of the dry face sheet is rather homogeneous, that of wet face sheet is highly heterogeneous and shows several changes in curvature. Despite the high amount of plastic deformation in the core, the I-webs did not delaminate from the face sheets with the exception of the small region reported in Fig. 7(c), which also corresponds to the large change in curvature mentioned above.

Figure 8 shows a view from the side of the panel before (a) and after (b) impulsive loading. These images clearly reveal that the core indeed crushed in the boundary between the water and air rings.

A second experiment was conducted on this sandwich geometry using a flyer plate 4.88 mm thick and an impact velocity of 301 m/s. This resulted in a peak pressure p_0 of 78.2 MPa and a characteristic decay time t_0 of ~26.1 μs. The corresponding applied impulse I_0 was 37.2 N s and the non-dimensional applied impulse $\hat{I}$ was 1.075. The maximum rear deflection was measured to be 10.53 mm and the non-dimensional maximum deflection, $\delta_{\max}/L$=0.138. The

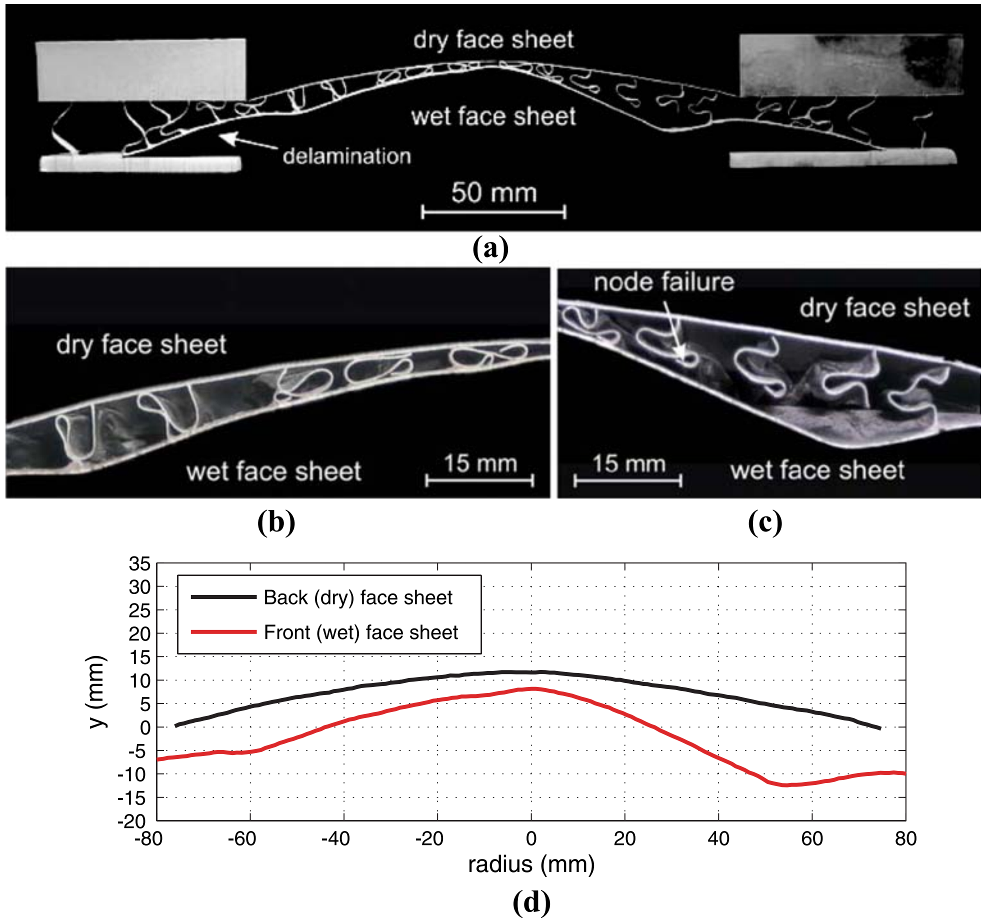

Fig. 7 (**a**) Cross-section of AISI 304 stainless steel sandwich panel with soft-I-core, case I (face sheets of equal thickness) after loading; (**b**) and (**c**) report details of the failure modes observed in the soft-I-core; (**d**) reports the post mortem profiles of the air and the water face sheets. (**a**) Cross-section, (**b**) detail of the cross-section, (**c**) detail of the cross-section, (**d**) post mortem face sheet deflection profiles

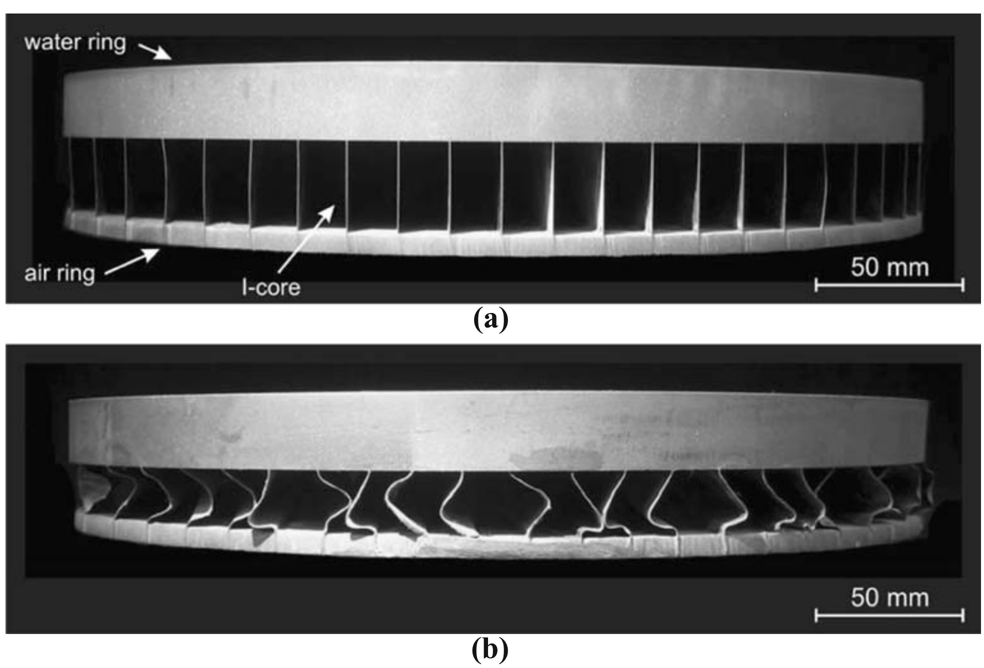

Fig. 8 Side view of AISI 304 stainless steel sandwich panel with soft-I-core, case I (sheets of equal thickness) before (**a**) and after (**b**) loading. (**a**) Before loading, (**b**) after loading

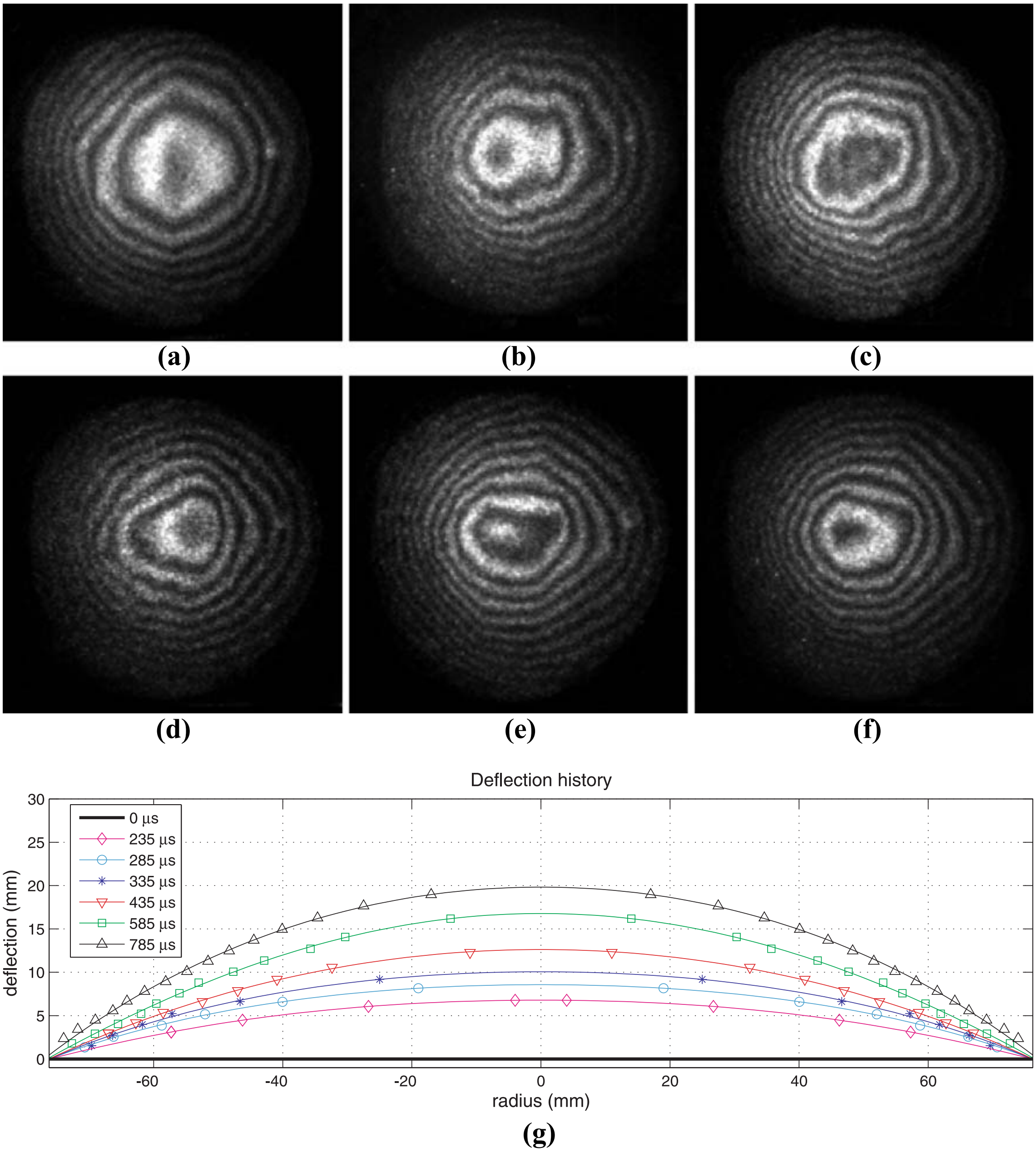

Fig. 9 (**a**)–(**f**) Sequence of high-speed camera images showing shadow moiré fringes for the AISI 304 stainless steel panel with soft-I-core and thick water face sheet; (**g**) deflection along the diameter of the specimen. Time t=0 μs corresponds to the arrival of the shock wave at the specimen location. (**a**) 235 μs, (**b**) 285 μs, (**c**) 335 μs, (**d**) 435 μs, (**e**) 585 μs, (**f**) 785 μs, (**g**) deflection history

observed failure modes were the same to those discussed above, therefore, repeatability of the panel performance was confirmed.

Case II: Thick Front Face Sheet

A panel with a thick from face sheet was tested using a flyer plate 4.98 mm thick shot and an impact velocity of 314 m/s. This resulted in a peak pressure p_0 of 81.5 MPa and a characteristic decay time t_0 of ~26.6 μs. The corresponding applied impulse I_0 was 39.51 N s and the non-dimensional applied impulse $\hat{I}$ was 1.141. The maximum rear deflection was 19.99 mm and, thus, the non-dimensional maximum deflection δ_{max}/L was 0.262.

Fringe patterns, obtained by Shadow Moiré and high speed photography, at six time instances between 235 and 785 μs after the wave front reached the specimen are shown in Fig. 9(a)–(f). The time at which the wave reaches the

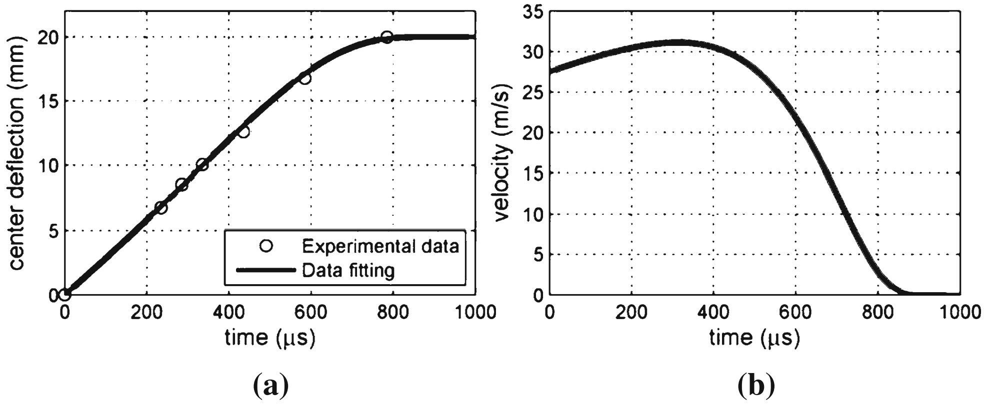

Fig. 10 History of the (**a**) maximum deflection and (**b**) velocity of the dry-face sheet for the AISI 304 stainless steel panel with soft-I-core and thick water face sheet. Time $t=0$ μs corresponds to the arrival of the shock wave at the specimen location. (**a**) Deflection history, (**b**) velocity history

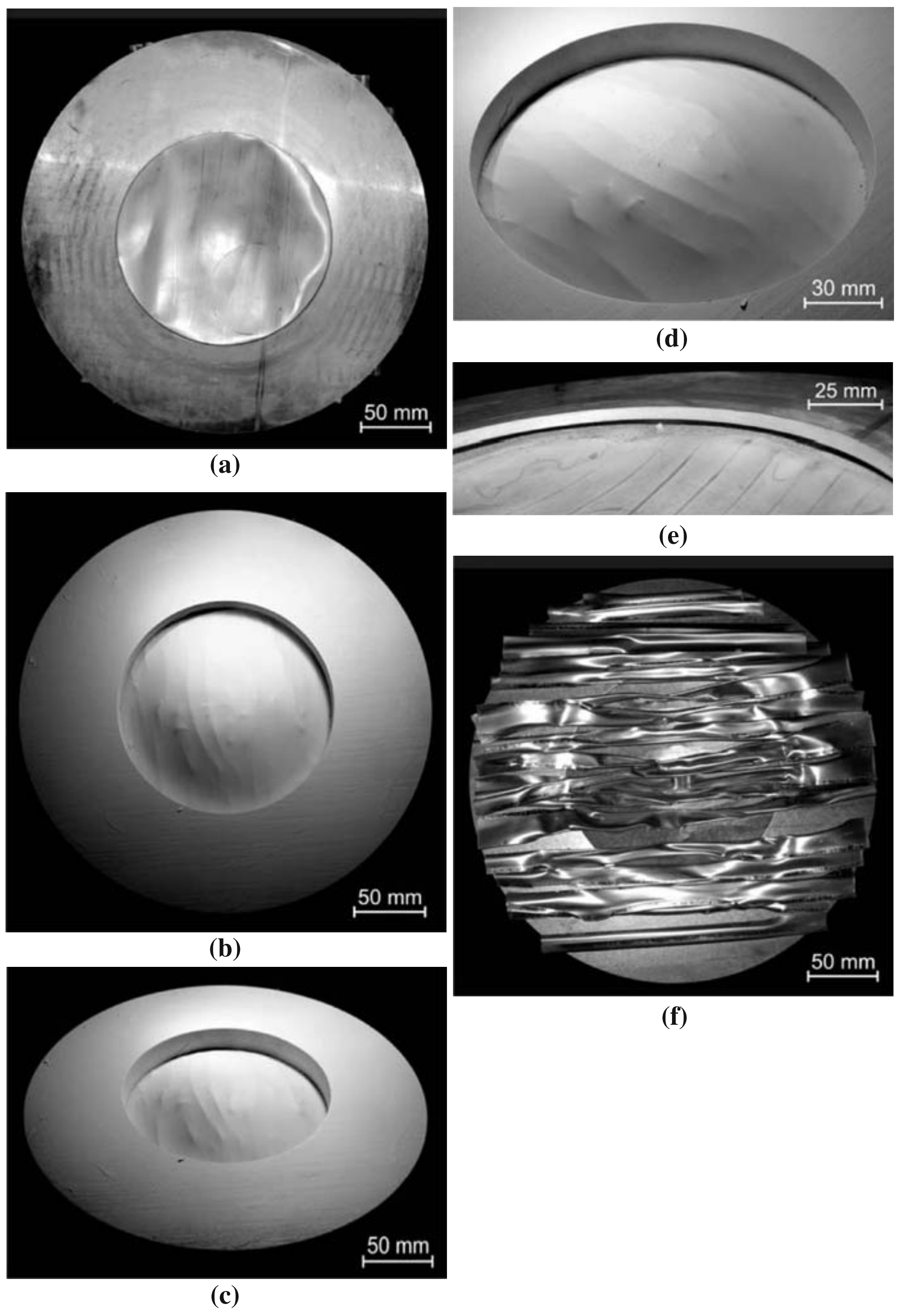

Fig. 11 Images of AISI 304 stainless steel sandwich panel with soft-I-core, case II (thicker wet face sheet), after loading; (**a**) and (**b**) show the front and the back of the face sheets; (**c**) shows an angled view; (**d**) reports a detail of the dry face sheet; (**e**) of the wet face sheet; and (**f**) shows a post-mortem view of the fully crashed core. (**a**) Front (wet side), (**b**) back (air side), (**c**) back side, (**d**) detail of the back, (**e**) detail of the front, (**f**) core

Fig. 12 Side view of AISI 304 stainless steel sandwich panel with soft-I-core, case II (thicker wet face sheet) after loading. Note massive core crashing and joint failure

specimen is predicted from finite element simulations, based on the model reported in [6], the geometry of the experimental set up, and the velocity trigger signal. Panel deflections along the diameter of the specimen are shown in Fig. 9(g). The history of the maximum deflection of the dry-face sheet, which occurred in the middle of the panel, is reported in Fig. 10. The velocity, reported in Fig. 10(b), is obtained as the first derivative of the continuous function that interpolates the displacement, Fig. 10(a). The maximum velocity at the middle of the panel is ~32 m/s.

The failure modes observed in this experiment are reported in Fig. 11. As for the specimen with equal face sheet thickness, a partial delamination occurred between the water face and the water ring, as shown in Fig. 11(e). The extent of the delamination was smaller than that observed for the case of face sheets of equal thickness. Due to the fact that the dry face sheet was 50% thinner than that of the sample with equal face sheets, it exhibited substantial imprints, as shown in Fig. 11(b)–(d). Note that the imprints are not exactly along straight lines, which may be the result of premature I-core and face sheet junction failure. The wet face sheet, which was 50% thicker than that of the sample with equal face sheets, showed very slight imprints, as shown in Fig. 11(a) and (e). Note that despite the massive core failure, the imprints did not lead to localized failure of the face sheets. The deformation of both the wet and dry face sheets was macroscopically homogeneous, due to the fact that the core was completely crushed, as shown in Figs. 11(f) and 12. The complete collapse of the core and massive junction failure caused the complete separation of the core from the face sheets as shown in Fig. 13.

Case III: Thin Front Face Sheet

As highlighted in the introduction, theoretical predictions [1, 8] point out to the fact that a panel mass distribution with lighter face sheets on the wet side should lead to enhanced performance. In this subsection we study such case under two normalized impulses to assess its effect on failure modes and overall performance.

High impulse ($\hat{I} = 1.1$)

The sandwich panel with a thin wet face sheet was tested using a flyer plate 5.11 mm thick launched at an impact velocity of 295 m/s. This resulted in a peak pressure p_0 of

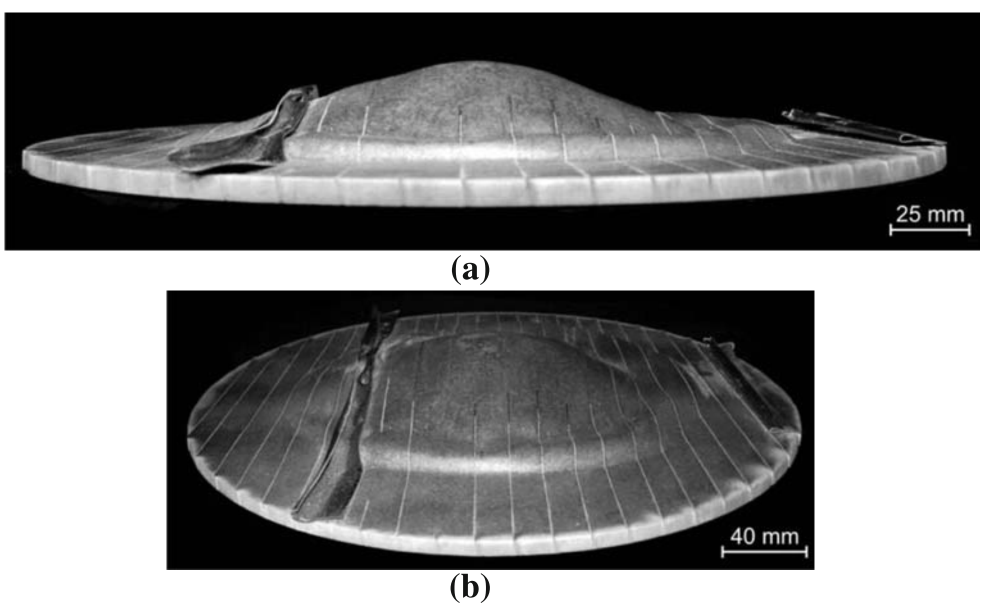

Fig. 13 Side view of the wet face sheet-ring assembly of the AISI 304 stainless steel sandwich panel with soft-I-core, case II (thicker wet face sheet), after impulsive loading. The wet face sheet-ring assembly was separated from the sandwich panel after the experiment since a complete separation between the face sheets and the I-webs had occurred

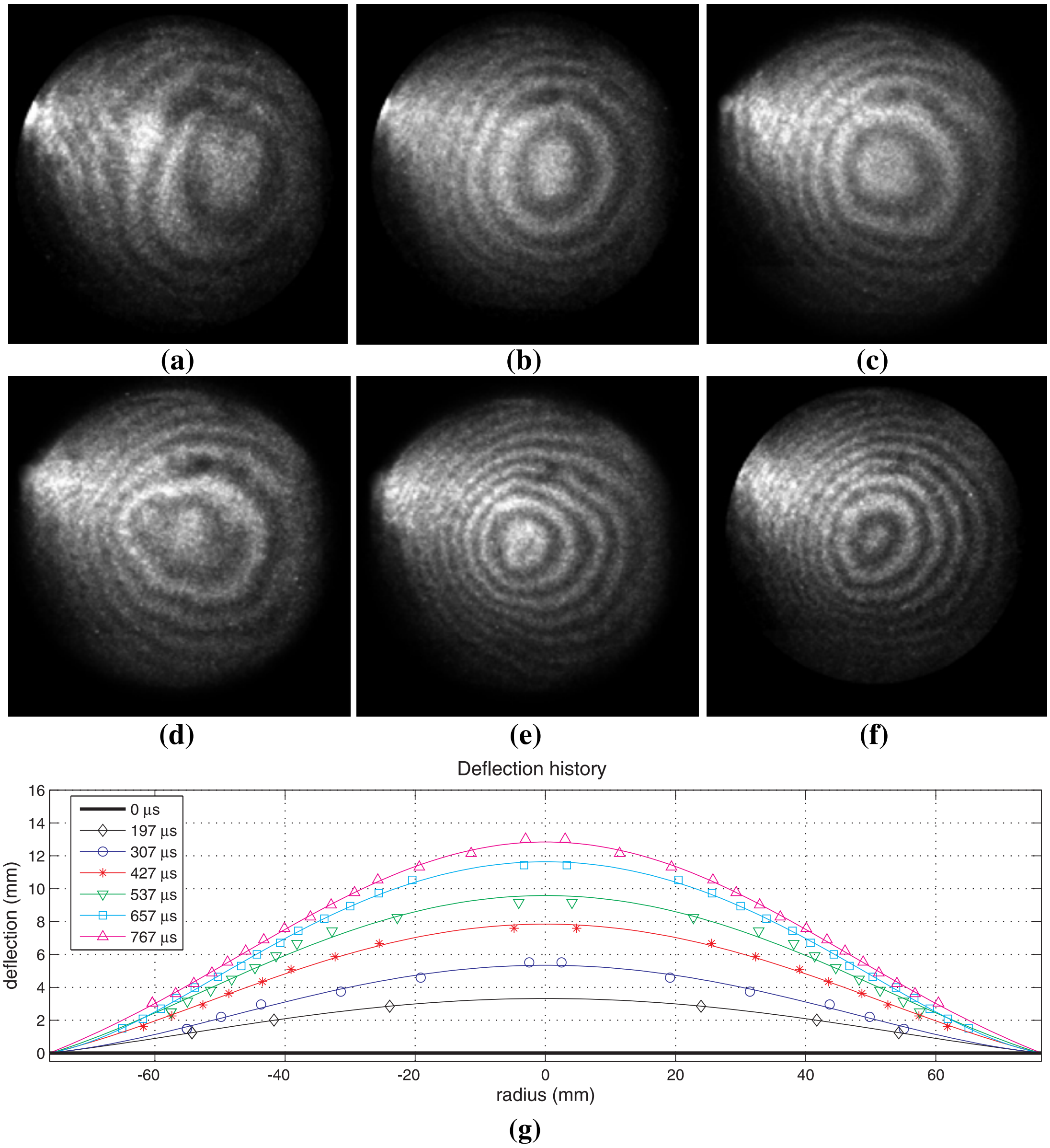

Fig. 14 (**a**)–(**f**) Sequence of high-speed camera images showing shadow moiré fringes for the AISI 304 stainless steel panel with soft-I-core and thin water face sheet subjected to a normalized impulse of 1.1; (**g**) deflection along the diameter of the specimen. Time t=0 μs corresponds to the arrival of the shock wave at the specimen location. (**a**) 197 μs, (**b**) 307 μs, (**c**) 427 μs, (**d**) 537 μs, (**e**) 657 μs, (**f**) 767 μs, (**g**) deflection history

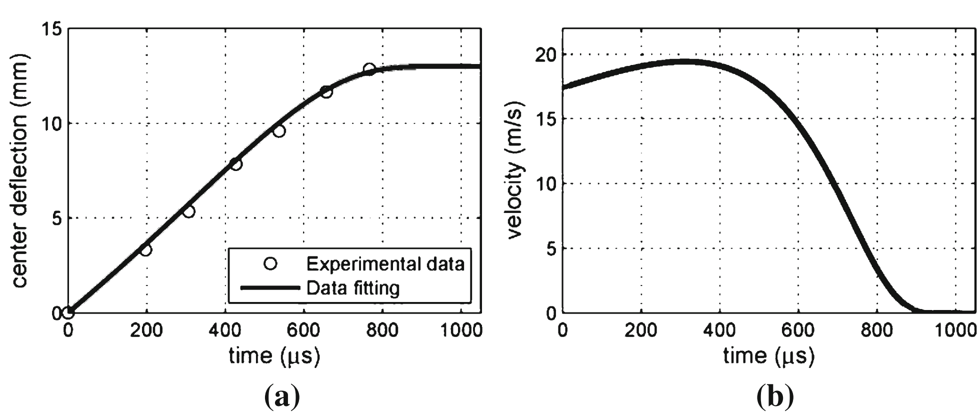

Fig. 15 History of the (**a**) maximum deflection and (**b**) velocity of the dry-face sheet for the AISI 304 stainless steel panel with soft-I-core and thin water face sheet subjected to a normalized impulse of 1.1. Time t= 0 μs corresponds to the arrival of the shock wave at the specimen location. (**a**) Deflection history, (**b**) velocity history

76.6 MPa and a characteristic decay time t_0 of ~27.3 μs. The corresponding applied impulse I_0 was 38.10 N s and the non-dimensional applied impulse $\hat{I}$ was 1.1. The maximum rear deflection was 12.98 mm and, thus, the non-dimensional maximum deflection δ_{max}/L was 0.17.

Fringe patterns, obtained by Shadow Moiré and high speed photography, at six time instances between 197 and 767 μs after the wave front reached the specimen are shown in Fig. 14(a)–(f). The corresponding panel deflections along the diameter of the specimen are shown in Fig. 14(g). The history of the maximum deflection of the dry-face sheet, which occurred in the middle of the panel, is reported in Fig. 15. The maximum velocity of the middle of the panel is 19 m/s and, as in the case of the panel with the thick front face sheet, it is reached about 310 μs after the wave front reached the specimen.

Figure 16 reports the observed failure modes in this experiment. In the case with equal face sheets, the sandwich

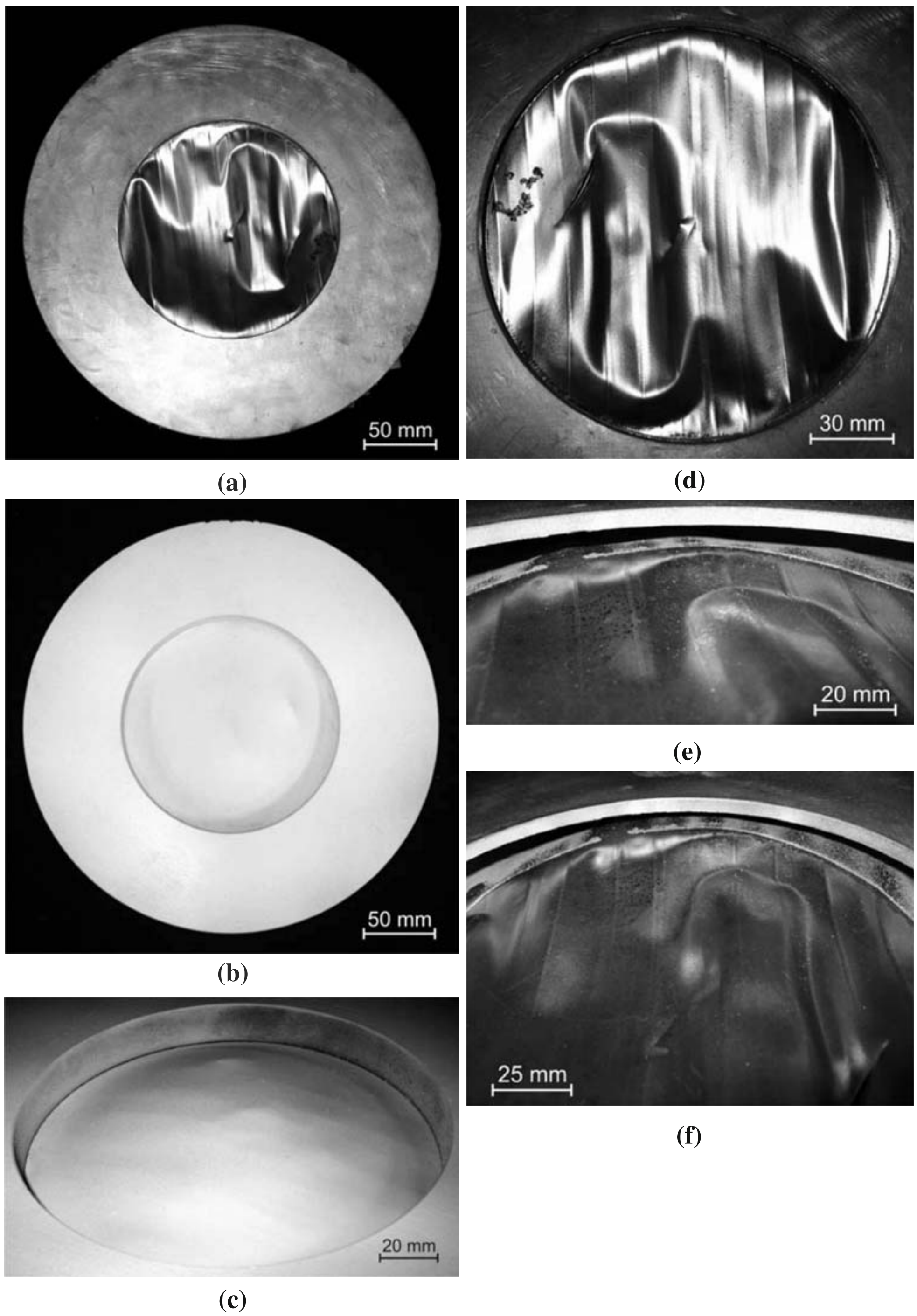

Fig. 16 Images of AISI 304 stainless steel sandwich panel with soft-I-core, case III (thicker dry face sheet), after the loading at high impulse; (**a**) and (**b**) show the front and the back of the plate; (**c**) shows a detail of the back; (**d**)–(**f**) details of the front. (**a**) Front (wet side), (**b**) back (air side), (**c**) detail of the back, (**d**) detail of the front, (**e**) detail of the front, (**f**) detail of the front

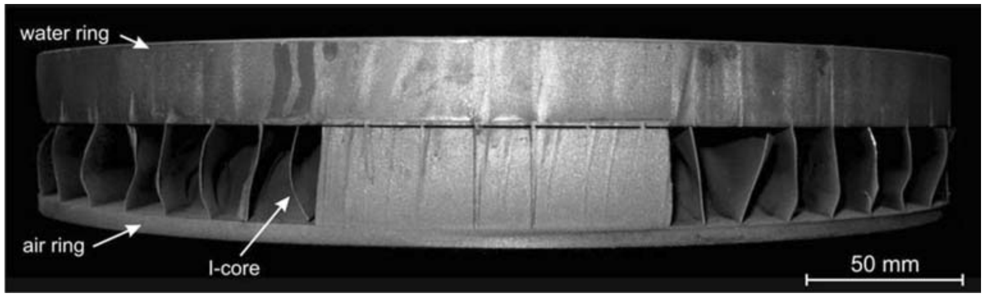

Fig. 17 Side view of AISI 304 stainless steel sandwich panel with soft-I-core, case III (thicker dry face sheet), after loading at high impulse

panel exhibited a difference in deformation behavior between front and back face sheets. In this case the difference was much more prominent. While the deformation of the wet face sheet was very heterogeneous, Fig. 6(a) and (d)–(f), that of the back face sheet was homogeneous, Fig. 16(c). Slight imprints appeared on the wet face sheet, which is 50% thinner than that of the case with equal face sheets, and very faint imprints appeared on the dry face sheet. As in the previous cases, a partial delamination occurred, between the wet face sheet and the water ring, as observed in Fig. 16(e) and (f).

Figure 17 shows a side view of the panel after impulsive loading. Some core crashing is observed at the boundary, between wet and dry face rings. The amount of core crashing is much smaller than that observed in the case of panels with face sheets of equal thickness.

After the experiment, the panel was sectioned and imaged as shown in Fig. 18. The wet face sheet exhibits a number of wrinkles and extensive delamination from the outer ring. Judging from the shape of the I-webs, it appears that almost complete core crashing occurred over the entire span of the sandwich structure. While junction failure occurred between the core and the wet face sheet almost all over the span of the panel, no failure is observed between the core and the dry face sheet. This is likely due to the fact that core crashing (web buckling) initiates on the wet side and that heterogeneous wet face sheet deformation occurred. A detailed numerical study is needed to elucidate the evolution of failure including the possibility of face sheets slamming as well as face sheet delamination. Geometric imperfections and joint strength are expected to play a significant role in the outcome of such analysis.

Low impulse ($\hat{I} = 0.734$)

Another panel with a thin wet face sheet was tested using a flyer plate 4.81 mm thick and an impact velocity of 209 m/s. This resulted in a peak pressure p_0 of 54.3 MPa and a characteristic decay time t_0 of ~25.7 µs. The corresponding applied impulse I_0 was 25.41 N s and the non-dimensional

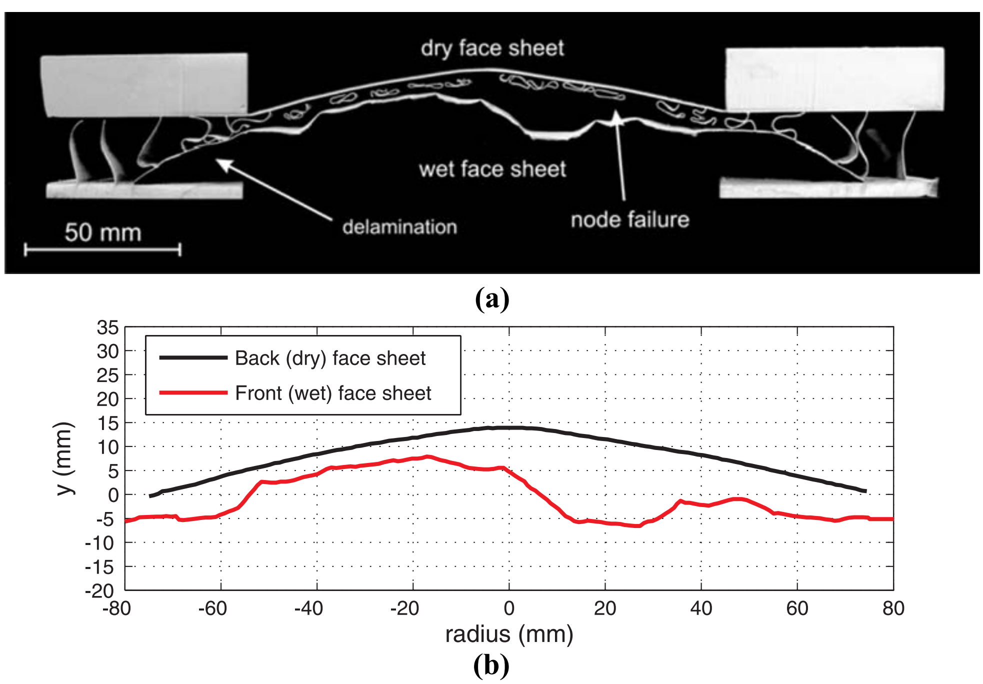

Fig. 18 (**a**) Cross-section of AISI 304 stainless steel sandwich panel with soft-I-core, case III (thicker front face sheet), after impulsive loading; (**b**) post mortem profile for air and water face sheets. (**a**) Cross-section, (**b**) post mortem face sheet profiles

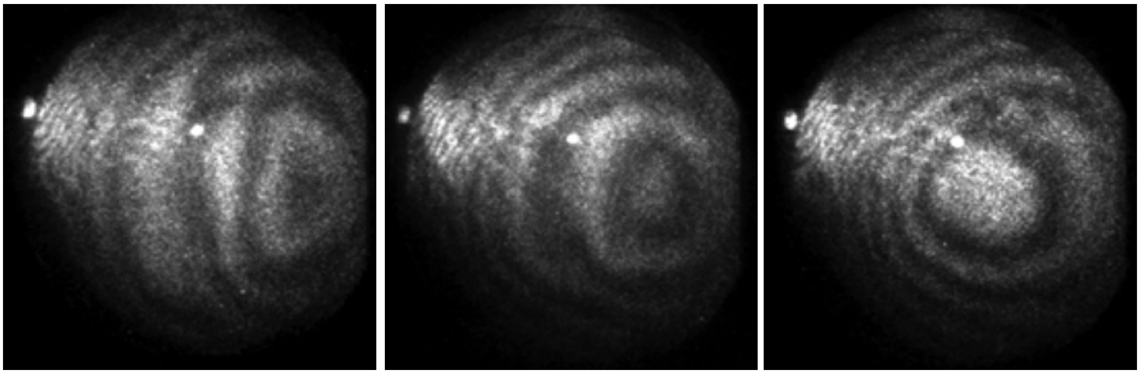

(a) **(b)** **(c)**

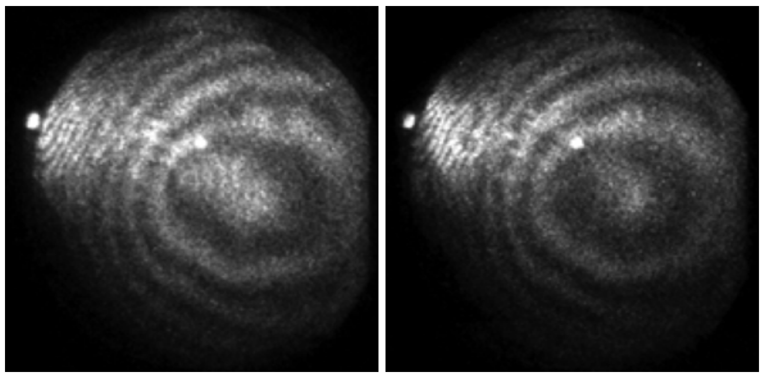

(d) **(e)**

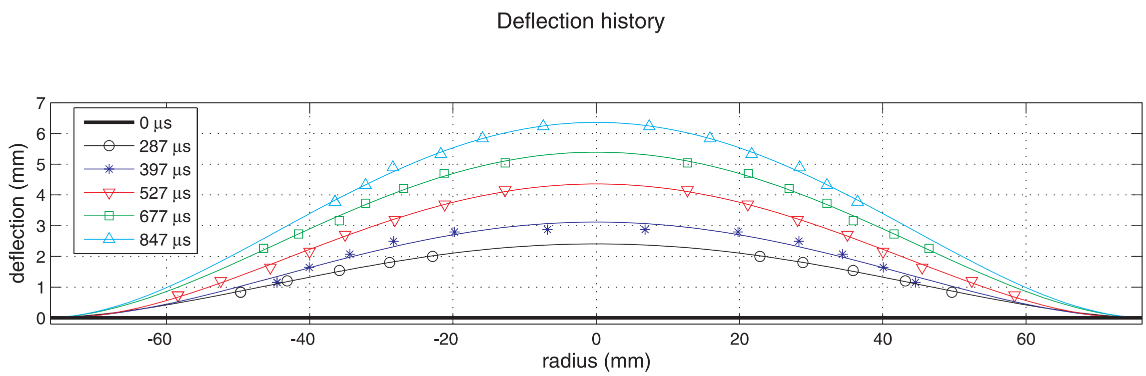

(f) deflection history

Fig. 19 (**a**)–(**e**) Sequence of high-speed camera images showing shadow moiré fringes for the AISI 304 stainless steel panel with soft-I-core and thin water face sheet subjected to a dimensionless impulse $\hat{I} = 0.734$, rand (**f**) deflection along the diameter of the specimen. Time t=0 μs corresponds to the arrival of the shock wave at the specimen location. (**a**) 287 μs, (**b**) 397 μs, (**c**) 527 μs, (**d**) 677 ms, (**e**) 847 ms, (**f**) deflection history

Fig. 20 History of the maximum deflection of the dry-face sheet for the AISI 304 stainless steel panel with soft-I-core and thin water face sheet subjected to non-dimensional impulse $\hat{I} = 0.734$. Time t=0 μs corresponds to the arrival of the shock wave at the specimen location. (**a**) Deflection history, (**b**) velocity history

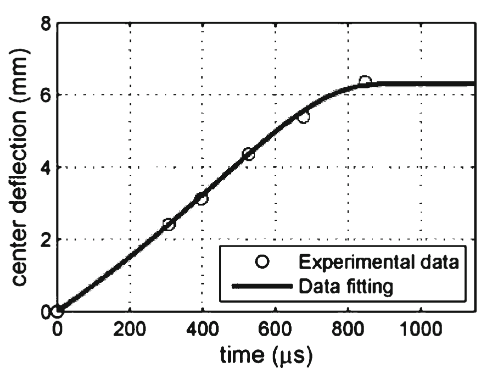

(a)

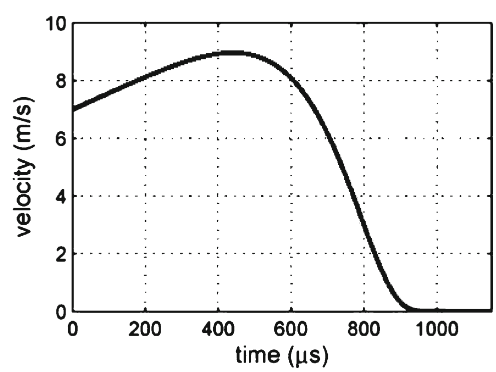

(b)

applied impulse $\hat{I}$ was 0.734. The maximum rear deflection was 6.32 mm and, thus, the non-dimensional maximum deflection δ_{max}/L was 0.083. The final strain of the core in the middle of the sample was estimated to be ε_c=61.7%.

Fringe patterns, obtained by Shadow Moiré and high speed photography, at six time instances between 287 and 847 μs after the wave front reached the specimen are shown in Fig. 19(a)–(e). The corresponding panel deflections

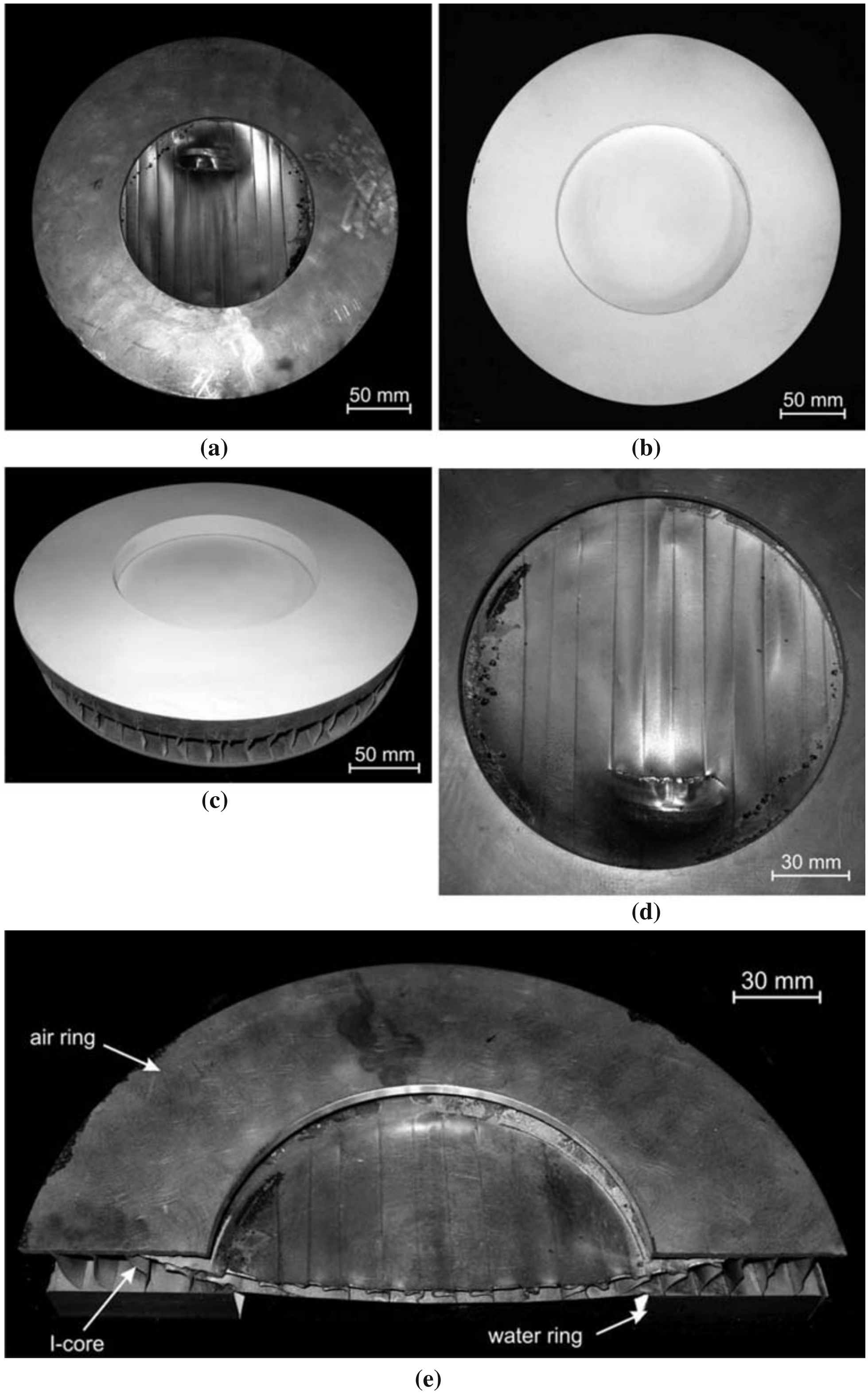

Fig. 21 Images of AISI 304 stainless steel sandwich panel with soft-I-core, case III (thicker dry face sheet), after impulse loading; (**a**) and (**b**) show the front and the back of the panel; (**c**) shows a side view; (**d**) and (**e**) report details of the front face sheet. (**a**) Front (wet side), (**b**) back (air side), (**c**) back side, (**d**) detail of the front, (**e**) detail of the front

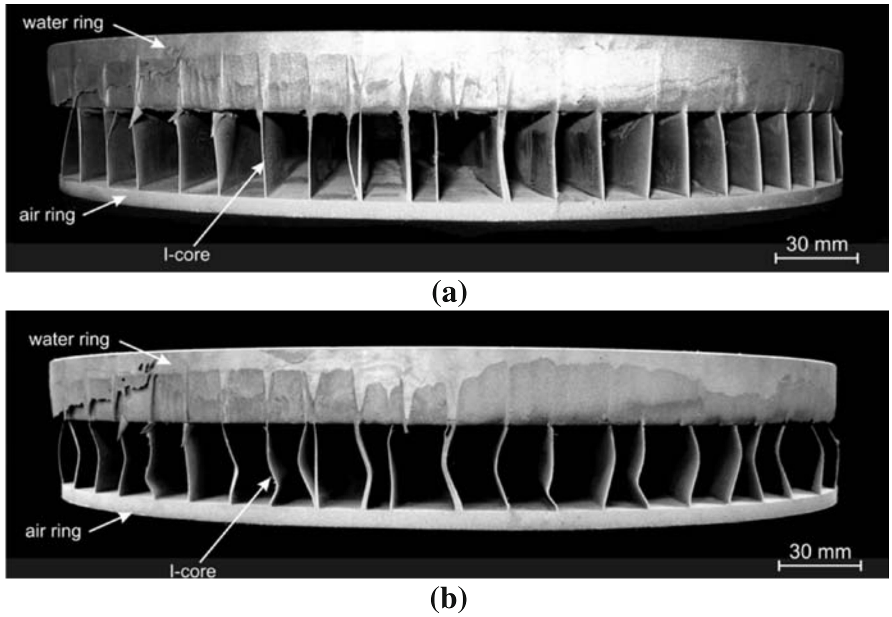

Fig. 22 Side view of AISI 304 stainless steel sandwich panel with soft-I-core, case III (thicker dry face sheet), before (**a**) and after (**b**) loading at low impulse. (**a**) Before loading, (**b**) after loading

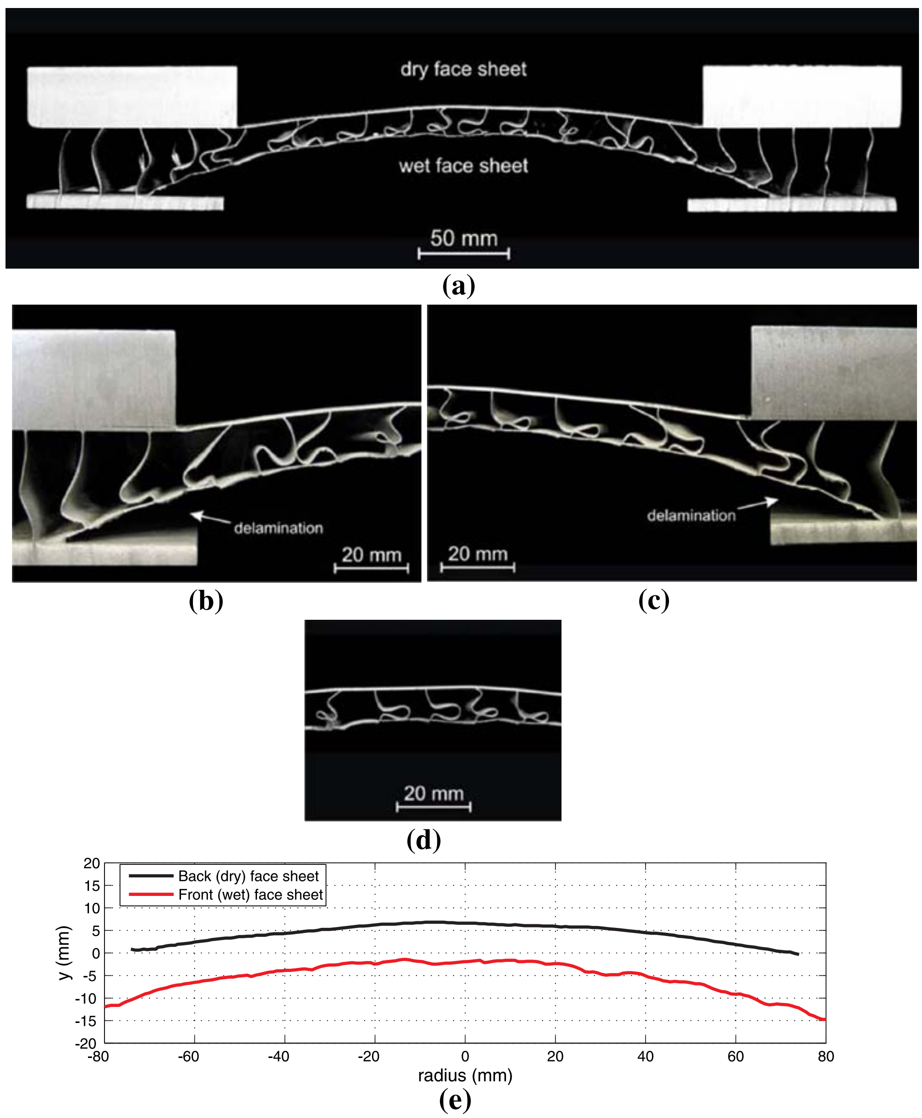

Fig. 23 Cross-section of AISI 304 stainless steel sandwich panel with soft-I-core, case III (thicker front face sheet), after loading at low impulse; (**b**)–(**d**) report details of (**a**) and shows the failure modes of the soft-I-core; (**e**) reports the post mortem profile for the air and the water face sheets. (**a**) Cross-section, (**b**) detail of the cross-section, (**c**) detail of the cross-section, (**d**) detail of the cross-section, (**e**) post mortem face sheet profiles

Table 3 Experimental conditions used in the testing of Soft-I-Core sandwich panels

Structure type	Impact velocity V_0 (m/s)	Flyer plate thickness t_f (mm)	Water pressure p_0 (MPa)	Characteristic decay time t_0 (μs)
Monolithic plate	298	4.97	77.31	26.53
Soft-I-Core, equal thickness	296	4.84	76.74	25.84
Soft-I-Core, thick wet face sheet	314	4.98	81.47	26.59
Soft-I-Core, thin wet face sheet	295	5.11	76.56	27.28
Soft-I-Core, thin wet face sheet	209	4.81	54.27	25.68

along the diameter of the specimen are shown in Fig. 19(f). The history of the maximum deflection of the dry face sheet is reported in Fig. 20. The maximum velocity in the middle of the specimen is ~9 m/s and is reached later than in the other experiments, about 450 μs after the wave front reached the specimen. Note that these maxima in displacement and velocity are about half of those measured for the dimensionless impulse $\hat{I} = 1.1$.

The failure modes observed in this experiment are reported in Fig. 21. In contrast to the case with higher impulse, the sandwich panel exhibited the same behavior for the front and the back face sheets: the deformation for both was homogeneous, Fig. 21(a)–(d). No imprints appeared on the dry face sheet and only slight imprints are observed on the wet face sheet except for a U-shaped imprint. This imprint is likely the result of the water piston hitting the sandwich panel very late in the experiment, i.e., after full panel deformation due to the water impulsive loading. Local damage to both the wet face sheet and the core are observed in Fig. 21(a) and (d). The damage, however, was much localized and did not affect the interpretation of the overall plastic deformation in the panel, as inferred from Fig. 21(e).

Figure 22 is a side view of the sample before and after impulsive loading. I-web buckling and core crashing at the boundary are observed, which is consistent with the boundary condition depicted in Fig. 2(b). The extent of boundary core crashing is similar to the one observed for $\hat{I} = 1.1$. As in all the other cases, a partial delamination occurred between the water face and the water ring, as shown in Fig. 23(a).

After the experiment, the panel was sectioned using water jet machining and imaged as shown in Fig. 23. The sample showed a homogeneous overall deformation in both face sheets. The slight waviness on the wet face sheet, visible in both Fig. 23(c) and (e), is due to the fact that the thin face sheet was bent by the impulse between each pair of supporting I-webs in the core. In the other experiments this behavior was not apparent because, either the core was completely collapsed or the wet face sheet was thicker. The core exhibits a homogeneous deformation all over the span and an earlier buckling stage when compared to all the other experiments. It is clear that the instability starts from the wet face sheet and propagates along the web towards the dry face sheet. The same behavior was previously observed for square honeycomb and pyramidal truss core sandwiches [9] as well as in the dynamic testing of I-webs [11, 12]. In contrast to the other two cases, no junction failure between core and face sheets was observed on either side. This suggests that junction failure at the web–water face sheet interface, observed for the higher impulse, is promoted by the full crashing of the core and the slamming between face sheets.

Comparison of Performances

In this section we compare the performance of the various cases based on the dimensionless impulse $\hat{I}$ given by equation (5) and the dimensionless maximum rear deflection, δ_{max}/L. The experimental conditions for each test are summarized in Table 3. Since the experiments were

Table 4 Experimental performances recorded for Soft-I-Core sandwich panels

Experiment	Final core strain ε_c (%)	Non-dimensional applied impulse $\hat{I}$	Non-dimensional maximum deflection δ_{max}/L	Normalized maximum deflection $(\delta_{max}/L)_N$	Improvement (%)
Monolithic plate	–	0.776	0.272	0.272	–
Soft-I-Core, equal thickness	87.5	1.045	0.153	0.114	58
Soft-I-Core, thick wet face sheet	–	1.141	0.262	0.178	34
Soft-I-Core, thin wet face sheet	–	1.100	0.170	0.120	56
Soft-I-Core, thin wet face sheet	61.7	0.734	0.083	0.088	68

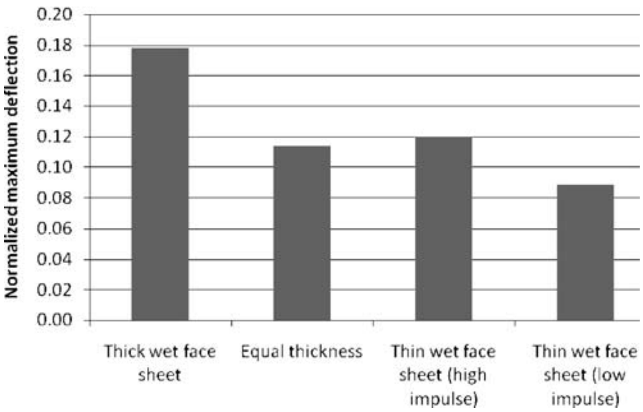

Fig. 24 Histogram of the normalized maximum deflection $(\delta_{max}/L)_N$ for soft-I-core panels with different face sheet thickness. All the specimens were made of AISI 304 SS

performed at slightly different non-dimensional impulses, all the results were referenced to the impulse applied to the monolithic panel. To scale the maximum deflection with impulse, we used the fact that non-dimensional deflection and impulse follow a linear relationship [3]. Then, the normalized maximum deflection is given by:

$$(\delta_{\max}/L)_N = I_{\mathrm{nf}} \times (\delta_{\max}/L) \tag{6}$$

where I_{nf} is the impulse normalization factor defined as:

$$I_{\mathrm{nf}} = \frac{\hat{I}_{\mathrm{monolithic}}}{\hat{I}}. \tag{7}$$

The calculations and improvements are reported in Table 4. It shows that all the tested panels exhibited significantly smaller panel deflection than the monolithic plate. As expected the panel with thicker wet face sheet exhibited the worst performance with an improvement of only 34% over the monolithic plate. Moreover, it showed complete collapse of the I-core-webs and failure of the junctions with the core. The structures with equal face sheet thickness showed the same performance at high impulse with an improvement of about 58%. The sandwich panel with thicker dry face sheet subjected to a low (non-densifying) impulse, however, exhibited the biggest improvement of 68%. Compared to pyramidal truss core and square honeycomb [9], the Soft-I-core shows better performance in terms of maximum deflection and never exhibited loss of impermeability due to fracture or tearing (as observed with the pyramidal hard cores [9]). These results are summarized in the histograms plotted in Figs. 24 and 25.

Concluding Remarks

An experimental study with the aim of quantifying performance and failure modes of sandwich structures, when subjected to impulsive loading, was conducted. In particular, performance enhancement with respect to solid panels of equal mass per unit area was assessed. Likewise, the optimal distribution of the mass per unit area in the design of sandwich structures was pursued by comparing the behavior of sandwich structures with various distributions of face sheets thickness.

By employing a previously developed FSI experiment, the study confirmed that usage of sandwich structures is beneficial and that performance enhancements as high as 68% are possible. As predicted by theoretical and computational analyses, the use of soft cores maximizes the benefits. However, while theory predicts that under equal normalized impulse further performance gains may be achieved by using unequal masses per unit area on the two face sheets, with the thicker in the back (air side), the experiments were unable to confirm such benefit. The discrepancy is likely related to the fact that the computational predictions did not include accurate stress/deformation levels for the failure of joints between the core webs

Fig. 25 Histogram of the normalized maximum deflection $(\delta_{max}/L)_N$ for different core geometries

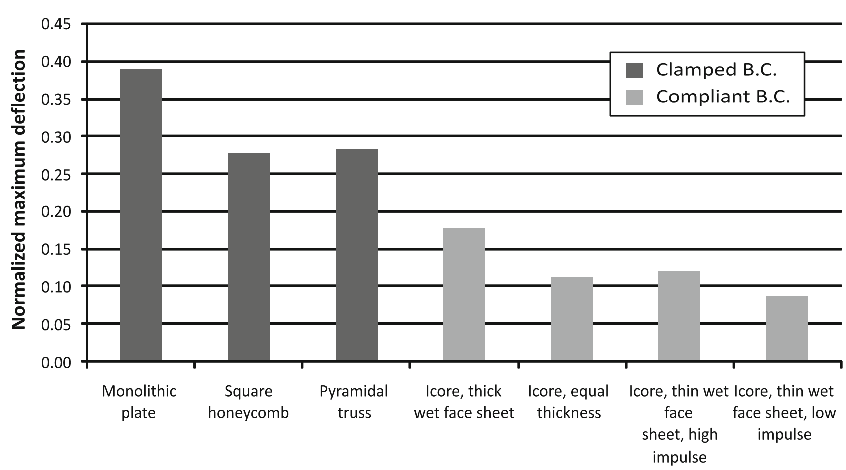

and the face sheets and to differences between experimental and computational boundary conditions. As discussed in the "Specimen Geometry and Boundary Conditions" section, the specimens were designed to reproduce as much as possible the compliant boundary condition used by Liang et al. [1]. However, the experimental observations revealed that the bonding between water ring and wet face sheet was not strong enough and exhibited delamination. This undesirable delamination affected the effective specimen span and probably the overall panel deformation. To reduce this effect, future investigations should be carried out to optimize the water ring mass, i.e., its thickness, in order to constraint the radial displacement while allowing as much as possible unrestricted core crashing.

Theory also predicts that thicker wet face sheet specimens exhibit a reduction in performance because of the fluid–structure interaction with a larger impulse being transferred to the structure in the early stages of deformation. This was confirmed by the present study.

Another interesting aspect revealed by this work is that the level of enhancement, with respect to solid panels of the same mass per unit area, is dependent on the applied normalized impulse, as illustrated in Table 4. Note that the same distribution of mass per unit area, between face sheets, resulted in different normalized maximum deflection for the same applied impulse. A better performance enhancement was achieved at lower impulses. Here again, failure modes and their sequence seem to be directly related to this finding. From the discussion of failure at low and high impact impulses, Figs. 14 and 23, one can infer that below a threshold normalized impulse, face sheet slamming and associated junction failure, at the web–face sheet interfaces, does not occur. This suggests the need for analytical models describing this phenomenon, which could be used in structure optimal design.

In closing, this work reveals a number of important features in the study of lightweight structures and points out to the synergies between structure geometry, materials, manufacturing methods, and threat level as manifested by the strength of the impulse. Further theoretical and computational studies accounting for experimentally observed failure modes and its interdependence with the fabrication methods is needed to achieve optimal performance designs and better predictive capabilities.

Acknowledgements This research was supported by the Office of Naval Research through MURI grant no. 123163-02-N00014-02-1-0700 to Harvard University, University of California at Santa Barbara, and Northwestern University (Program Manager Dr. R. Barsoum) and awards N00014-01-1-1051 to the University of Virginia and N00014-07-1-1139 to Northwestern University (Program Manager Dr. D. Shifler).

References

1. Liang Y, Spuskanyuk AV, Flores SE, Hayhurst DR, Hutchinson JW, McMeeking RM, Evans AG (2007) The response of metallic sandwich panels to water blast. J Appl Mech 74:81–99.
2. Hutchinson JW, Xue ZY (2005) Metal sandwich plates optimized for pressure impulses. Int J Mech Sci 47:545–569.
3. Xue ZY, Hutchinson JW (2004) A comparative study of impulse-resistant metal sandwich plates. Int J Impact Eng 30:1283–1305.
4. Deshpande VS, Fleck NA (2005) One-dimensional response of sandwich plates to underwater shock loading. J Mech Phys Solids 53:2347–2383.
5. Fleck NA, Deshpande VS (2004) The resistance of clamped sandwich beams to shock loading. J Appl Mech 71:386–401.
6. Espinosa HD, Lee S, Moldovan N (2006) A novel fluid structure interaction experiment to investigate deformation of structural elements subjected to impulsive loading. Exp Mech 46:805–824.
7. Lee S (2005) Dynamic failure of blast-resistant structures subjected to impulsive loading. Ph.D. Thesis, Northwestern University, Evanston, IL, USA
8. Wei Z, Deshpande VS, Evans AG, Dharmasena KP, Queheillalt DT, Wadley HNG, Murty Y, Elzey RK, Dudt P, Chen Y, Knight D, Kiddy K (2008) The resistance of metallic plates to localized impulse. J Mech Phys Solids 56:2074–2091.
9. Mori LF, Lee S, Xue ZY, Vaziri A, Queheillalt DT, Dharmasena KP, Wadley HNG, Hutchinson JW, Espinosa HD (2007) Deformation and fracture modes of sandwich structures subjected to underwater impulsive loads. J Mech Mater Struct 2:1981–2006.
10. Smith PD, Hetherington JG (1994) Blast and ballistic loading of structures. Butterworth-Heinemann, Oxford.
11. Radford DD, Fleck NA, Deshpande VS (2006) The response of clamped sandwich beams subjected to shock loading. Int J Impact Eng 32:968–987.
12. Rathbun HJ, Rodford DD, Xue ZY, He MY, Yang J, Deshpande VS, Fleck NA, Hutchinson JW, Zok FW, Evans AG (2006) Performance of metallic honeycomb-core sandwich beams under shock loading. Int J Solids Struct 43:1746–1763.